Jurnal Manajemen Hutan Tropika, *32*(3), 215–228, July 2026
EISSN: 2089-2063
DOI: 10.7226/jtfm.32.3.215

Scientific Article
ISSN: 2087-0469

Estimation of Stand Volume Using Empirical Modeling Based on Multi-sensor Imagery with Random Forest Regression

Galih Citra Yogyanti[1], Projo Danoedoro[2], Sanjiwana Arjasakusuma[2]

[1]Department of Geography, Faculty of Mathematic and Natural Science, Universitas Negeri Makassar, Jl. Mallengkeri Raya No. 44, Parang Tambung, Makassar, Indonesia 90224
[2]Department of Geographic Information Science, Faculty of Geography, Universitas Gajah Mada, Jalan Kaliurang, Bulaksumur, Yogyakarta, Indonesia 55281

Received July 9, 2025/Accepted November 12, 2025

Abstract

Stand volume estimation is the process of measuring the volume of tree stands, which serves as an indicator of forest ecosystem structure and biomass. This assessment supports various applications, including the implementation of reduced impact logging, a sustainable forest management strategy that employs selective harvesting based on tree maturity to preserve ecological integrity. However, measuring resources in large, complex forests with limited access is challenging for detailed resource measurement. This study was conducted in Central Kalimantan Province, as one of the production forest land uses with a naturally growing silviculture system. Forest canopy density (FCD) is employed to determine the classification of field samples. Furthermore, multi-sensor imagery was employed to derive input variables for stand volume estimation. Among the 19 predictors, the most influential were the FCD transformation, GEMI, and SAVI indices from Sentinel-2, along with bands 12 (SWIR) and 5 (red edge). Results indicated that variables derived from passive sensors contributed most significantly to the accuracy of the volume estimation model. The optimal stand volume estimation model generated from multi-sensor images had an R^2 value of 0.824 and RMSE of 9.7 at m-try 4 and n-tree 100. Estimation of stand volume using random forest obtained results in each sample plot size of 30 m^2 plots ranging from 0.05 m^3 to 55.4 m^3.

Keywords: *natural production forest, FCD model transformation, Sentinel-1, Sentinel-2*

**Correspondence author, email*: *galih.citra@unm.ac.id*

Introduction

Periodic comprehensive inventories are crucial for natural forest use to ascertain areas for various permits. Stand volume estimation, which includes measuring tree volume, has strategic objectives such as implementing reduced impact logging (RIL) for forest sustainability and providing information about carbon storage, biodiversity, economic value, and ecosystem benefits. RIL helps reduce damage and monitor production impacts, while stand volume inventories provide important information about tree regeneration, stand stock, and forest productivity. By limiting the cutting diameter for each annual works plan in the primary forest, the remaining stands can recover after 35 years (Heriansyah et al., 2022). Furthermore, the implementation of RIL not only minimizes physical damage to the forest but also facilitates systematic monitoring of production-related activities such as area clearing and silvicultural interventions like fertilization, which directly influence stand recovery, regeneration dynamics, and long-term forest productivity. Estimating stand volume also has other strategic value, including being able to assess carbon absorption and climate change mitigation (Giri Ananto et al., 2019). Stand volume inventories can also be used to estimate forest value in terms of timber or non-timber forest products (NTFPs) as well as potential economic benefits from recreation or ecosystem services. The most significant and accurate variables that influence forest stand productivity can be assessed from the abundance of tree regeneration, remaining stands, and potential reflected in the stand density, basal area, and stand volume (Manan et al., 2019). Variables including stand density, basal area, and commercial tree volume influence productivity, and technologies namely digital hemispherical photography support productivity estimates, especially in natural forest areas.

Large, complex forest areas and limited access pose significant challenges for detailed resource measurements. The use of remote sensing and the integration of geographic information science makes it easier to map and inventory forest resources in terms of time, cost, and data accuracy. The success of remote sensing methods hinges on the availability and currency of data, as well as image processing tailored to regional characteristics that can yield accurate and useful results (Abdollahnejad et al., 2017). Forest canopy density (FCD) is an index transformation that uses a combination of advanced vegetation index (AVI) and bare soil index (BSI) with principal component analysis (PCA). It also uses a combination of the thermal index and scale shadow index (SSI) derived from the shadow index (SI) and initially processed into the advanced shadow index (ASI) using linear transformation. Using these four index transformations, FCD can describe information about vegetation cover by suppressing the influence of soil backgrounds and shadows from Landsat TM data (Roy et al., 1997; Rikimaru et al., 2002). It provides information on vegetation feature space stratified based on texture, which is influenced by canopy shadow (Roy et al., 1997). Therefore, the final results of FCD are implemented to achieve vertical classification of land cover and forest density with a combination of indices that increase the separation of vegetation and non-vegetation areas. The extent of canopy cover is an important indicator of the health and biodiversity of an ecosystem measured using satellite imagery, aerial photography, or field surveys. Furthermore, the relationship between FCD and wildlife habitat is very close; forests provide habitat for a variety of fauna species, and the density of cover can have a major impact on the diversity and abundance. Some tree species require a certain minimum amount of canopy cover to survive, while others may thrive in more open environments with direct sun exposure (Giertych et al., 2015).

Trends, data sets, methods, and frameworks used in forest stand volume estimation studies have been widely investigated both with medium spatial resolution imagery using Landsat 8 imagery (Shehzad et al., 2022) and radar (Ataee et al., 2019), as well as the use of unmanned aerial vehicles (UAV) (Brede et al., 2022). Given that remote sensing techniques cannot directly capture forest structural attributes, research commonly relies on empirical models that establish relationships between field plot inventory data and remote sensing-derived metrics, using either univariate or multivariate analytical approaches. Therefore, this study was conducted to examine the ability of FCD to classify forest structures used in estimating stand volume in production. Empirical modeling was also carried out using field data from the results of the FCD classification, the Sentinel-2 vegetation index, and polarization from Sentinel-1.

The use of Landsat optical images with thermal channels for the FCD model provides an initial classification based on canopy density, a development of the guide that uses unsupervised classification in field classification. FCD, the result of index transformation, is used for forest rehabilitation planning, degradation monitoring, and reforestation progress. It maps changes in land cover, such as those that occur in natural production forest over 10 years, reflecting degradation due to selective logging and changes in land cover from reforestation. The application in canopy density classification provides a basis for estimating stand volume, which is important for understanding the influence of production activities and the success of regeneration. Land cover changes using multi-temporal imagery with FCD models have been widely carried out (Himayah et al., 2016; Ismail et al., 2017). Active and passive remote sensing, such as radar and multispectral imagery, are expected to estimate stand volume by providing information about forest structure and composition. This method, especially the random forest algorithm, allows the development of universal models for broader estimates and increases the precision of forestry data through the integration of multi-sensor information (Esteban et al., 2019; Iizuka et al., 2020). Unlike most FCD studies conducted in natural forests (Sukarna, 2008; Mas Sukarna & Syahid, 2015; Himayah et al., 2016; Ismail et al., 2017; Salsabila & Danoedoro, 2021). This research was carried out in a production forest environment in Central Kalimantan with high cloud cover and characterized by intensive management and structural heterogeneity. These conditions demand tailored integration between passive (Sentinel-2) and active (Sentinel-1) data to accurately estimate canopy density and volume. Based on the problems and questions described, The primary aim of this study is to evaluate the applicability of the FCD model for canopy classification within production forest conditions. In particular, the research focuses on identifying the most relevant predictor variables and optimizing the Random Forest Regression model to enhance the accuracy of stand volume estimation derived from multisensor remote sensing data.

Methods

Study area in this study was conducted at Wana Inti Kahuripan Intiga LLC is a company that has a forest utilization business license or *perizinan berusaha pemanfaatan hutan* (PBPH), with a working area of ±92,475 ha. Geographically, this study area was located at coordinates S015–035 latitude and E11445–11450 longitude with an altitude of 30 to 200 m above sea level (m asl). Most of the concession areas were in the moderately steep (35.50%) to steep (31.86%) slope class, but there were no very steep slopes. This study used the main material in the form of medium-resolution remote sensing images, namely Landsat 8 OLI/TIRS Level 1, Sentinel-2, and Sentinel-1 images, DEM SRTM for the topographic correction. In addition, other secondary data were used to fulfill the study objectives such as periodic comprehensive forest inventory or *inventarisasi hutan menyeluruh berkala* (IHMB) table on 2019 and the boundary of study area. The flowchart shown in Figure 1 provides a clear visualization of the process.

Pre-processing Landsat-8 Topographic correction is required to reduce the influence of sunlight on the same object to ensure that objects in the valley and hill areas have relatively similar colors and hues. It also shows the difference between vegetation and open-ground objects more clearly (Salsabila & Danoedoro, 2021). The extraction of topographic information is carried out on SRTM DEM images to calculate the incident angle between the normal angle and sunlight. In this study, the topographic correction method used was C-correction. This method is non-Lambertian and Performed by employing a semi-empirical equation using pixel illumination values and solar angles (Umarhadi & Danoedoro, 2020). Furthermore, geometric correction aims to improve the position of pixels by referring to the map based on the principle of a correct projection and coordinate system (Danoedoro, 2012). The corrected image was also re-corrected geometrically by the image-to-vector method through the rectification of Landsat 8 images recorded in 2020 against the boundary of the concession. In addition, this is also intended to be carried out later to cut the image and provide focus on the appropriate study boundary.

In this study, the image used was the Landsat-8 OLI-2/TIRS-2 on path/row 118/60, recorded on February 22, 2020. The image was selected because it had the least cloud

EISSN: 2089-2063 ISSN: 2087-0469
DOI: 10.7226/jtfm.32.3.215

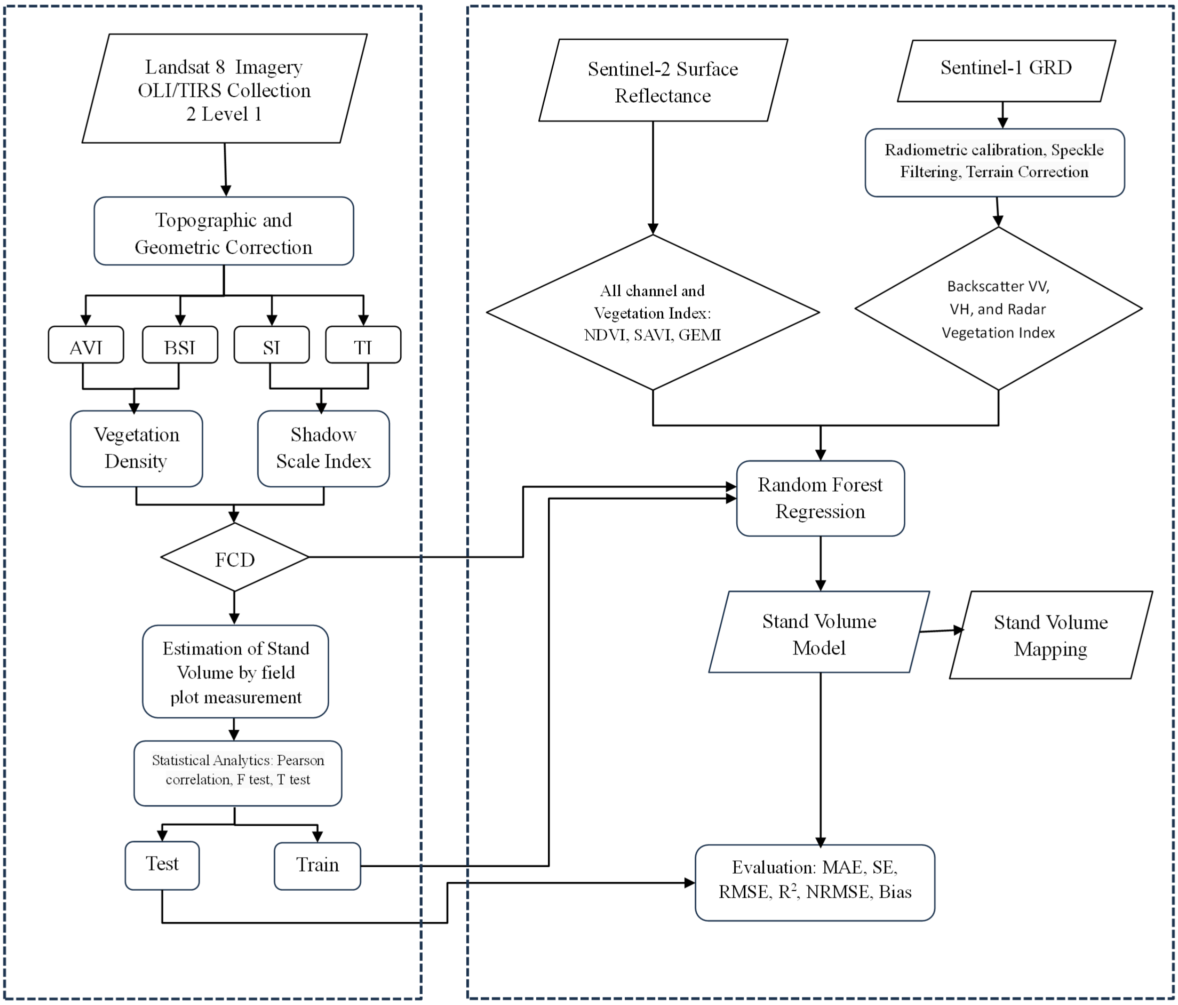

Figure 1 Flowchart.

disturbance in the area. The pixel value (brightness value) in each image channel recorded by the sensor describes the strength of different reflected energy and has the ability to detect the minimum as well as the maximum spectral radiance of an object on the earth surface (Danoedoro, 2012). Atmospheric correction was performed using the dark object subtraction (DOS) method, assuming that water bodies have zero reflectance. The result is a corrected image having a value between 0 and 1.

Data from each channel of the Landsat-8 image needs to be adjusted to the appropriate range because, in the FCD model, the formulated data must have a range of 8 bits (0–255). This was ensured to follow the FCD transformation equations performed by Rikimaru et al. (2022) (Equation 1 to Equation 6). In addition, FCD mapper software in this study requires an 8-bit data format with a range of 0–255 to avoid needing a large amount of memory for storage and speed up the data processing process. The FCD model transformation is a method used to identify the structural composition of a forest using Landsat OLI images with four indices, as follows (Rikimaru et al., 2002).

Vegetation index was derived from the AVI to show chlorophyll a by normalizing the NIR and red channels, which can be calculated using Equation *[1]*.

$$AVI = \sqrt{((NIR + 1) \times (256 - Red) \times (NIR - Red))} \qquad [1]$$

Bare soil index (BSI) is an index used to suppress the background soil by using the middle infrared, blue, and red channels, which can be calculated using Equation *[2]*. The values are converted to 8-bit with a range of 0 to 255.

$$BSI = \frac{(SWIR1+Red) - (NIR+Blue)}{(SWIR1+Red) - (NIR+Blue)} \qquad [2]$$

The shadow index (SI) is a method of using spectral information from forest shadows and thermal information influenced by the presence of canopy shadows, which can be calculated using Equation *[3]*. The index is a step in extracting low spectral radiance from visible spectral channels.

$$SI = \sqrt[3]{((256 - Blue) \times (256 - Green) \times (256 - Red))} \qquad [3]$$

The thermal index represents surface temperature values derived from the thermal infrared band, obtained by converting radiance values, which can be calculated using

Equation *[4]* and Equation *[5]*.

$$L_\lambda = (Gain \times DN) + Bias \quad [4]$$

$$T = \frac{K2}{ln\left(\left(\frac{K1}{L_\lambda}\right)+1\right)} \quad [5]$$

note: L_λ = radiance of the warmest pixel in the scene/(m²srμm); $Gain = \frac{L_{max} - L_{min}}{DN_{max} - DN_{min}}$; DN = digital number; Bias = min; T = surface temperature value (°C); $K1$ = 666.09 watt/(m² m ster μm); $K2$ = 1,282.71 watt/(m² m ster μm).

Principal component analysis (PCA) is used to generate vegetation density (VD) from the combination of two indices, namely AVI and SI with a negatively strong correlation. VD is the result of a new image that is valued in the range of 0% to 100%. Black soil detection is processed through shadow and thermal index. SI is spatially processed into previously ASI to produce the percent forest shadow. Normalization through linear transformation results in the SI being rescaled to 0–100 representing 0–100% cover, namely the scale shadow index (SSI). Regions with an SSI value of 0 corresponded to areas with no shadow presence (SI = 0), while areas with an SSI value of 100 indicated complete shadow coverage, representing 100% shadow intensity. The four indices are then integrated into the FCD model using Equation *[6]*.

$$FCD = \sqrt{(VD \times SSI + 1)} - 1 \quad [6]$$

Pre-processing Sentinel-1 In this study, Sentinel-1A imagery with an acquisition date of September 7, 2023 was processed and downloaded through Google Earth Engine (GEE). SLC interferometric wide swath data collected in the descending pass direction, which captured data with dual polarization (VV and VH) backscatter was used. In this setup, electromagnetic waves are vertically polarized (V) for transmission and horizontally or vertically polarized (H/V) for reception. Previously, Sentinel-1A images were processed with radiometric slope correction, one of which is optimized for vegetation applications by assuming volume scattering on the surface and showing increased radar backscatter in mountainous areas (Vollrath et al., 2020). Speckle noise removal was then performed with the Lee Sigma method based on the sigma probability of the normal distribution. This type of calibration defines radar backscatter at the ground area reference based on the earth ellipsoid model. The sigma standard deviation of the whole scene was first calculated and then each central pixel in the moving windows was replaced with the mean of the surrounding pixels having intensities within the sigma range of the central pixel. Therefore, the presence of speckles in synthetic aperture radar (SAR) images must be reduced before further analysis is carried out using the Lee Sigma filter (Medasani & Reddy, 2018; Yu et al., 2018; Rao, 2023). Resampling was carried out from the pixel size of the Sentinel-1 image (10 m) to a size of 30 m. This resampling was conducted to align with the spatial scale of field plots and ancillary datasets, ensuring consistency in pixel-based analysis and reducing speckle variability. This approach prioritizes operational coherence over fine-scale structural enhancement, and while texture or fusion-based methods were not applied, the chosen resolution was deemed sufficient for canopy cover estimation in heterogeneous terrain. This is consistent with findings from Mullissa et al. (2021), who emphasized the importance of harmonizing SAR data resolution for vegetation analysis in GEE workflows, and Rubela et al. (2020), who demonstrated the predictive reliability of Lee filtering in Sentinel-1 imagery. Medasani and Reddy (2018) further support the use of Lee Sigma filtering for speckle reduction in medium-resolution SAR datasets, validating its effectiveness in preserving structural integrity during preprocessing. The result of this process was backscatter from VV and VH polarizations characterized by speckle noise removal (σVH and σVV) with a pixel size of 30 m.

Three predictor variables were extracted in Sentinel-1, consisting of VV and VH polarization backscatter and the radar vegetation index (RVI), an index used as predictor variables. Nasirzadehdizaji et al. (2019) used an alternative formulation using dual-pol Sentinel-1 data (VV VH), where

$$RVI = \frac{4\sigma VH}{\sigma VV + \sigma VH} \quad [7]$$

RVI can be used to monitor vegetation multi-temporally, similar to the use of normalized difference vegetation index (NDVI) throughout the season, and the spectral reflectance pattern is not saturated. However, RVI cannot replace NDVI simply because it cannot represent the greenness value. The acquisition of biophysical parameters from RVI is essential (Kumar et al., 2013).

Pre-processing Sentinel-2 This study used Sentinel-2 level 2A, an image that has been geometrically corrected globally using GCP and DEM. The data collected were the surface reflectance values, while the image used was already available in the form of atmospherically, radiometrically, and geometrically corrected data. The resampling method was carried out on Sentinel-2 images with a spatial resolution of 30 m to overcome the difference in resolution with other variables from Sentinel-1 and the results of FCD transformation. A total of 110 Sentinel-2 images from January 2019 to September 2023 were downloaded through GEE, with the selected images already in the surface reflectance and cloud masking process. In this study, 50 m × 50 m plots were used, fulfilling the assumption of a plot size appropriate to the Kucler vegetation type. This requirement was fulfilled to prevent underestimation of field data collection results. Accordingly, in volume estimation models using multisensor imagery, actual tree volume is calculated from individual tree diameter and height measurements within the field plots, which are then generalized to a 30 m × 30 m spatial resolution.

In this study, 12 channels owned by Sentinel-2 and vegetation indices were used, including the basic vegetation index (NDVI), as well as indices that suppress atmospheric (GEMI) and soil background influence (SAVI). The reflectance of the 12 channels owned by Sentinel-2 and the vegetation indices were then compared quantitatively regarding the response to vegetation objects in the images. A seasonal median reducer was utilized across all Sentinel-2

Jurnal Manajemen Hutan Tropika, *32*(3), 215–228, July 2026
EISSN: 2089-2063
DOI: 10.7226/jtfm.32.3.215

ISSN: 2087-0469

image scenes to extract representative seasonal optical features for classification purposes. This function effectively generates a cloud-free dataset by filtering out noisy pixels, thereby enhancing data quality and consistency (Ghorbanian et al., 2021). NDVI was selected as a vegetation index for volume estimation due to the ability to effectively describe vegetation variations despite atmospheric effects and sensor degradation. This ability is attributed to the normalization process, which reduces calibration issues. However, It exhibits sensitivity to variations in viewing and illumination geometry, particularly in areas characterized by low vegetation density, and tends to overestimate vegetative cover at the start of the growth season and underestimate at the end (Bannari et al., 1995; González-Alonso et al., 2006; Zhu & Liu, 2015). NDVI transformation is represented in Equation *[8]*.

$$NDVI = \left(\frac{NIR-RED}{NIR+RED}\right) \qquad [8]$$

Soil-adjusted vegetation index (SAVI) suppresses the influence of soil reflectance values by adding the variable L, which represents the soil surface condition index. The equation for calculating SAVI is as shown in Equation *[9]*.

$$SAVI = \frac{((NIR-Red)(1+L))}{(NIR+Red+L)} \qquad [9]$$

Pinty and Verstraete (1992) proposed an alternative approach, which consists of reducing different indices designed to minimize the relative influence of atmospheric effects. The equation is as shown in Equation *[10]*.

$$GEMI = \eta\,(1 - 0.25\,\eta) - \frac{(RED-0{,}125)}{(1-RED)} \qquad [10]$$

note: $\eta = ((2\,(NIR^2 - RED^2)) + 1.5\,NIR + 0.5\,RED)/NIR + RED + 0.5$

Preparation for field survey The objective of stratification using satellite imagery is to divide the area proposed for inventory into smaller and more homogeneous units to improve the accuracy of the results based on the condition of stand density. The classification of stand density is carried out through the rule of dividing up all existing vegetation cover (exhaustive) and combining classes (mutually exclusive). The number of samples was determined using the stratified random sampling method based on FCD class. ASPRS in Congalton and Green (2019) stated that the minimum number for remote sensing is 20, but samples can be added according to the increase in the area. As stated by Kuchler and Zonnevald (988), the selection of sample size has two aspects, namely the appropriate number to obtain reliable statistical data and the plot size to represent the classification unit (vegetation type). The comparison between the transformed value of the FCD model and canopy cover from the field survey showed significant differences attributed to structural changes at the study site in the last three years. The selection of the model entailed modeling without plots not used due to differences between the results of image analysis and the actual condition caused by field changes at a time close to field data collection, with a total of 60 samples divided into 30 models and 30 accuracy test samples.

The plot size takes into consideration both the spatial resolution of the imagery and the root mean square error (RMSE) value from the geometric correction of the image. Based on the RMSE values obtained from the geometric correction process, a sample size of 60 m × 60 m was determined. Therefore, data collection in this study follows the technical guidance for IHMB plots from the Ministry of Environment and Forestry, which are square plots measuring 50 m in length and 50 m in width. These dimensions closely match the image resolution and effectively represent the vegetation classification units (Kuchler & Zonnevald, 1988). Essentially, this pertains to a forest composition structure with a smaller plot size in accordance with the classification unit (vegetation type). The requirement is essential to prevent the collection of underestimated data. Samples collected during field activities were divided into two categories, namely model and accuracy test. The division was made by comparing the model and accuracy test samples based on the total that can be achieved in the field, using a 50%:50% ratio.

Field survey Field data collection was carried out from 7 July to 19 July 2023 with a total of 70 measurement plots collected from an initial plan of 104 plots. This was due to limited access to forest areas, clearing difficult terrain, and also weather factors. Measurement plots were taken according to the distribution of density classification results from the FCD model transformation of Landsat 8 imagery, which is assumed to represent all classes. The distribution of sample points is shown in Figure 2 and Table 1.

Sampling was carried out in areas that could be reached at each value of VD from the FCD class with stratified random sampling. Height measurements were carried out on all trees present in the sample plot for later volume determination based on a geometric method to calculate the volume of all species stands (all species) consisting of trees with a diameter at breast height (dbh) equal to or greater than 10 cm (ten

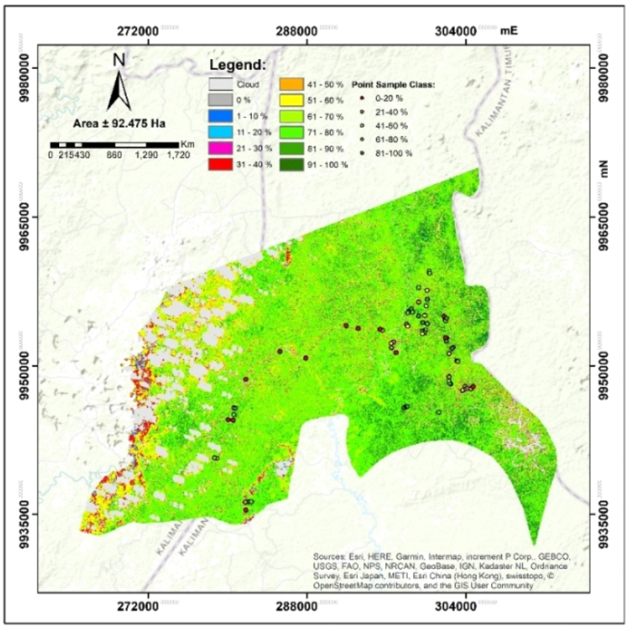

Figure 2 FCD model transformation.

Jurnal Manajemen Hutan Tropika, *32*(3), 215–228, July 2026
EISSN: 2089-2063
DOI: 10.7226/jtfm.32.3.215

ISSN: 2087-0469

centimeters). Furthermore, data from hemispherical photography were processed to calculate the canopy density of each sample. Binary classification was used, comprising vegetation objects and non-vegetation. Other information taken in the field includes understory and land cover at the sample location, such as forest, shrub, grass, or non-vegetation.

Field data were collected by visiting the planned plots from the reclassification of FCD classes into five classes. Using GPS, the azimuth points were drawn from the edge of the main road to the center coordinates. In the 50-m square plots, data collected included corner coordinates, plant diameters above 10 cm, free branch tree height, tree species identification, and actual density with an upward photo taken. Hemispherical photographs are very sensitive to lighting conditions, and the background must be standardized for the canopy to accurately distinguish without bias (Díaz, 2023). Accordingly, image acquisition followed a grid-based layout encompassing all cardinal directions, a total of nine points including the center of the plot (Figure 3). The camera was positioned at a stable mean height for each sample and processed with a gap light analyzer (GLA) (Frazer et al., 1999).

Post-field statistical analysis Normality test was performed on both modeled and accuracy samples. The correlation between the FCD model and reference (canopy cover) showed a positive correlation, with an increase in canopy cover corresponding to a rise in spectral values. Table 2 shows the value of regression statistics using 30 samples. Canopy density estimates were obtained from a simple linear regression equation applied to the transformed FCD model.

Table 1 Forest canopy density (FCD) class

FCD class	Area (ha)	Number of point
0–20%	11,336.79	15
21–40%	2,966.52	8
41–60%	11,025.42	13
61–80%	55,087.34	19
81–100%	12,141.03	15
Total	92,557.10	70

T-test and *F*-test were also conducted in the regression analyses to determine whether the model samples passed the significance threshold. The statistical value for the FCD transformation and the significance of the *F*-value was 0.000 (p-value < 0.05), indicating that the independent variable partially affects the dependent variable. In regression analysis, the t-statistic assesses whether there is a partial effect of the independent variable on the dependent. In addition, the R^2 value represents the coefficient of determination, which assesses whether the model is effective. It also shows a stronger correlation compared to the original dataset without removing outliers. This level of accuracy can convey precise information about the type of structure composition based on natural forest and avoid overestimating values. Overestimation potentially occurs in forests with high heterogeneity in canopy cover density (Nasiri et al., 2022). Canopy density estimates were obtained through simple linear regression, and accuracy was tested using the standard error of estimates (SEE), RMSE, and MAE methods as presented in Table 3.

Empirical models using random forest Random forest algorithm was used in data mining to select the most optimal variables through iteration (model tuning). Some points assessed based on variables include fairness, robustness, and causality. Random forest is a non-linear machine learning algorithm that can be used for classification or regression. In this context, random forest regression is formed by growing trees depending on the random vector θ; hence, the tree predictor $h\ (x,\theta)$ takes a numerical value as opposed to the class label. The output value is numerical and the training set is taken independently from the distribution of random vector Y, X. The m-square generalization error for the numerical predictor is as shown in Equation *[11]*.

$$h(x) = E_{X,Y}(Y\text{-}h)X))^2 \qquad [11]$$

The requirement for accurate random forest regression includes a low correlation between residuals and errors at low trees. Random forest reduces the mean error of the used trees by a factor of ρ and the randomization must lead to low correlation (Breiman, 2001). Compared to previous simple

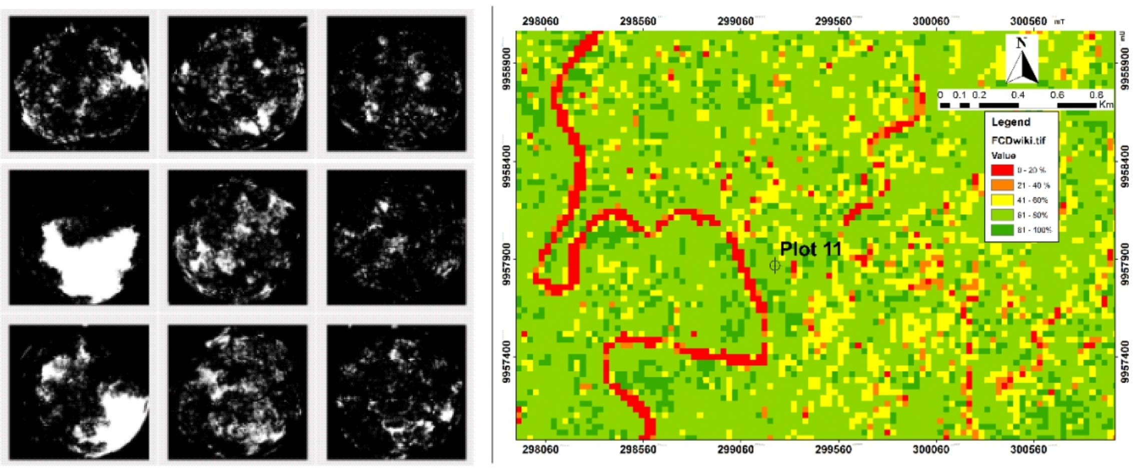

Figure 3 Hemispherical photography of plot 11 with ferns understory.

Jurnal Manajemen Hutan Tropika, *32*(3), 215–228, July 2026
EISSN: 2089-2063
DOI: 10.7226/jtfm.32.3.215

ISSN: 2087-0469

Table 2 Regression statistic values

	FCD
r	0.93
R^2	0.86
F-value	0
t-stat	13.23
t-value	0
A	3.21
B	1.09
Pearson correlation	0.91

Table3 Accuracy results of canopy density estimation from FCD transformation

	FCD
Sum	10,967.40
Mean	65.93
Stdev	39.17
Cl 95%	14.02
Upper range	79.95
Lower range	51.92
Max error	38.12
Min error	24.76
Max accuracy	75.24
Min accuracy	61.88
SEE	19.79
RMSE	19.12
MAE	13.97

empirical or semi-empirical models, random forest can create more flexible and accurate models based on measurement data in the field. Firstly, the analysis explicitly allows for nonlinear relationships between dependent and independent variables. These methods do not make a priori assumptions about the distribution of the data, as well as the relationship between independent variables, or the dependent and independent variables. Secondly, the analysis is well suited to handle nonhomogeneous data sets such as unbalanced sample size and high variability. The results are also easy to interpret and the predictive power of each independent variable is explicit (Kalkhan, 2011; Schratz et al., 2019; Wittke et al., 2019). In this study, the random forest was used to develop a regression model that connects the reflectance values of Sentinel-2 satellite images, Sentinel-1 images, and FCD transformation with the most optimal variables from field data.

Results

Correlation result of FCD and field data Using FCD Mapper, NDVI, advanced normalized vegetation index (ANVI), and AVI showed a correlation of 0.76, 0.66, and 0.59 with BSI, respectively. Furthermore, NDVI was used as the preferred input for the establishment of VD. The FCD model shows different characteristics of various indices, including AVI, BI SI, and TI. This model can provide an indication of forest growth and the degree of density. Figure 4 shows all the indices used in building the FCD model.

The land cover of production forest in the study area varies, including sparse with a dry swampy understory that has low FCD values, but the density of forest in the study area also varies. The actual canopy taken upward can result in a dense canopy reading. Other land cover includes unused skid trails overgrown with pioneer plants, namely the Mahang tree (*Macaranga gigantea*), one of the most widespread species in southeast Asia, and ferns locally known as Jangang (*Dicranopteris linearis*), making the FCD model read a dense density layer. Land cover in the form of open land consists of tree cuts on either side of the road, logpound, and labor camps.

Sentinel-2 vegetation index The dominant factors affecting vegetation spectral reflectance in blue and red wavelengths are absorbed by vegetation for photosynthesis, while green wavelengths are reflected, and near-infrared wavelengths are highly reflected by healthy leaves. Transformation of vegetation indices such as NDVI, SAVI, and GEMI was performed to show vegetation objects. The statistical values of the transformed indices show variation depending on the index type, with NDVI having smaller variations than GEMI and SAVI.

Table 4 shows the statistical values of the index transformation result. NDVI has values between -0.222 to 0.921, and a pattern mostly close to the maximum value with a mean of 0.828. These values are influenced by saturation in very dense vegetation. The GEMI index values ranged from -0.087 to 1.268 with a mean of 0.495 and SAVI with a minimum value range of -0.056 to 0.691. The GEMI index and SAVI tend to depict a more even distribution pattern due to the ability to minimize the influence of atmospheric and ground reflections. The smaller the standard deviation, the more similar the index transformation values. In a previous study comparing the use of vegetation indices (Rondeaux et al., 1996), GEMI had a low direct sensitivity to soil. This result is presumably due to the high sensitivity of the index to soils with very low vegetation cover. A very low sensitivity was obtained with GEMI, which may be a soil response related to canopy interactions. SAVI has a slightly higher sensitivity but is more constant over the whole range of land cover; hence, this index would be better for vegetation classification.

Sentinel-1 variable SAR imagery shows visual differences between near-range and far-range, influenced by geometric distortion and the incident angle of microwave radiation. Near-range objects look closer due to the lower angle of incidence. Forest vegetation shows a medium-tone appearance because the radar pulse is scattered and partially reflected to the sensor on the aircraft. The VV polarization range has a minimum value of -12.623 dB to 2.434 dB, while the VH polarization value ranges from 18.575 dB to -4.851 dB. The difference between both channels in radar backscatter is that VV generally has higher levels than VH (Villarroya-Carpio et al., 2022). In SAR images with VV and VH polarization, forest vegetation shows a medium tone due to the backscatter of radar waves. The difference between VV and VH is influenced by the dielectric properties of vegetation. Vertical polarization is more sensitive to plant biomass, while horizontal is more sensitive to the vegetation canopy. However, with cross-polarization, VH will be more

Jurnal Manajemen Hutan Tropika, *32*(3), 215−228, July 2026
EISSN: 2089-2063
DOI: 10.7226/jtfm.32.3.215

ISSN: 2087-0469

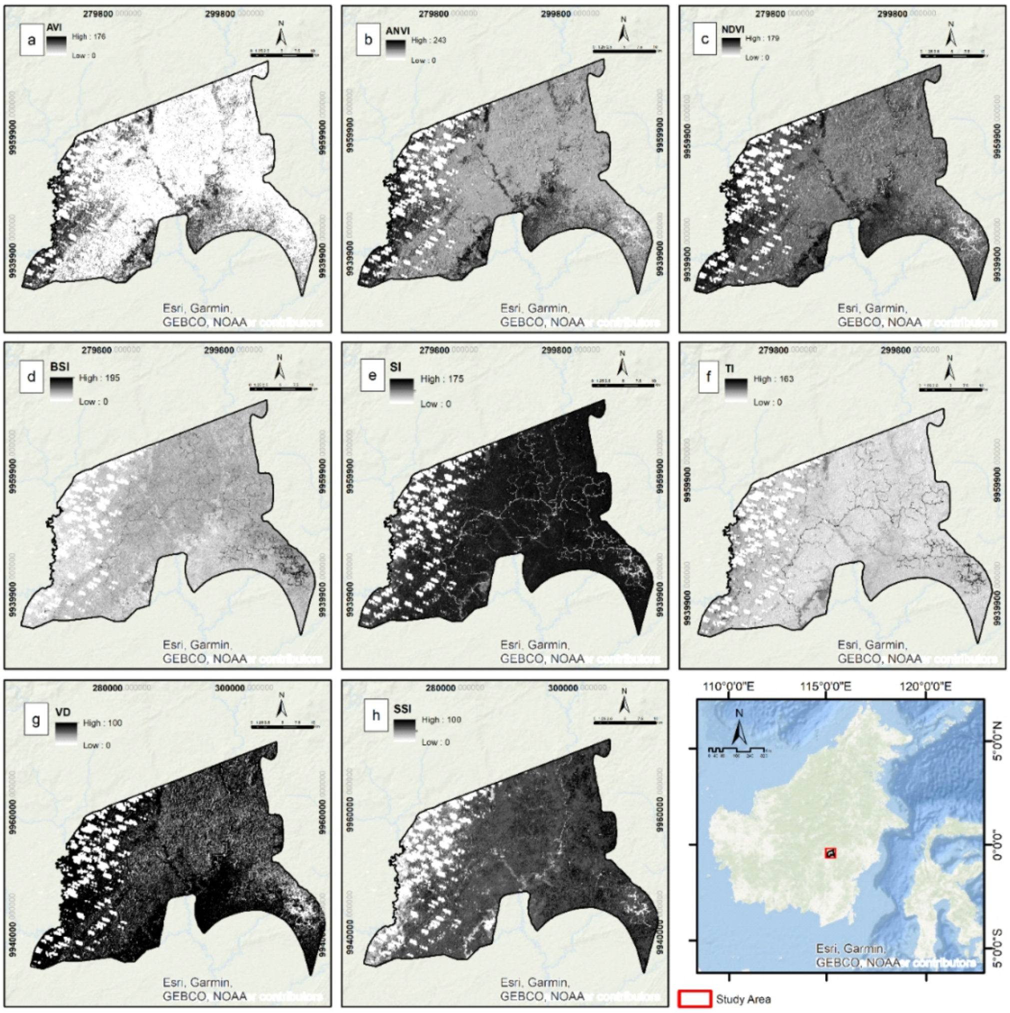

Figure 4 Example of the Landsat 8 OLI-based indices used to build the FCD model. In this figure, all indices were processed using atmospheric correction and topographic correction. AVI (a), ANVI (b), NDVI (c), BSI (d), S I(e), TI (f), VD (g), and SSI (h).

Table 4 Transformed value of vegetation index from Sentinel-2A

Index	Min	Max	Mean	StDev
NDVI	-0.222	0.921	0.828	0.066
GEMI	-0.087	1.268	0.495	0.099
SAVI	-0.056	0.691	0.460	0.059

sensitive to the vegetation canopy (Kumar et al., 2013; Szigarski et al., 2018).

RVI is calculated based on the radar backscatter value, with a high value indicating the presence of dense vegetation. Sentinel-1 has dual polarization in VV and VH with RVI index values in the C-band found in the range of 0 to 1 according to plant growth conditions (Yadav et al., 2022). The RVI index also follows the phenological stage of the crop and depicts the development of the crop canopy. It is a vegetation index that can be used to measure volume estimation. Production forests with the selected silviculture system or *tebang pilih tanam Indonesia* (TPTI), have heterogeneous vegetation cover characteristics both in terms of species and age, causing RVI values to vary from a minimum value of 6.83754e-06 to a maximum value of 0.833. Furthermore, RVI can be used for monitoring natural production forests by measuring changes in values over time. These changes may indicate alterations in forest conditions, such as land cover, vegetation growth, and degradation.

Hyperparameter tuning Hyperparameter tuning is a modeling result evaluation mechanism to adjust the parameters of machine learning. In this study, the Random Forest Regression method was used to produce better models. The evaluation was carried out by setting the n-tree and m-try parameters in 20 different scenarios. Each scenario has m-try (2, 3, 4, and 5) and n-tree values (100, 200, 300, 400, and 500) on all samples divided into 70% for training and 30 % for validation as shown in Table 5. The best model selection was based on threshold fluctuations in the m-try and n-trees parameters in training data, as well as taking into account R^2 and RMSE values. The accuracy measurement using RMSE was selected because it provided an overview of global errors, including outliers, to determine the general

Jurnal Manajemen Hutan Tropika, *32*(3), 215–228, July 2026
EISSN: 2089-2063
DOI: 10.7226/jtfm.32.3.215

ISSN: 2087-0469

Table 5 Hyperparameter tuning for training data

Hyperparameter tuning		Data test					
SPLIT	TREES	SE	RMSE	nRMSE	MAE	bias	R^2
2	100	10.873	10.616	21.925	7.778	-10.568	0.792
2	200	10.926	10.669	22.033	7.768	-10.582	0.799
2	300	10.897	10.640	21.973	7.729	-10.603	0.800
2	400	10.911	10.655	22.002	7.722	-10.595	0.804
2	500	10.840	10.585	21.860	7.709	-10.583	0.809
3	100	10.296	10.054	20.763	7.275	-11.026	0.818
3	200	10.334	10.091	20.839	7.200	-11.006	0.815
3	300	10.290	10.048	20.750	7.199	-11.025	0.819
3	400	10.247	10.006	20.664	7.156	-10.961	0.822
3	500	10.213	9.973	20.595	7.164	-10.837	0.826
4	100	9.941	9.707	20.046	6.845	-11.251	0.824
4	200	9.966	9.731	20.096	6.903	-11.090	0.826
4	300	9.977	9.742	20.118	6.930	-11.115	0.828
4	400	9.936	9.702	20.036	6.891	-11.052	0.831
4	500	9.925	9.691	20.013	6.893	-11.077	0.833
5	100	9.908	9.675	19.979	6.840	-11.224	0.829
5	200	9.826	9.595	19.814	6.736	-11.048	0.832
5	300	9.793	9.563	19.747	6.781	-11.101	0.835
5	400	9.797	9.567	19.756	6.763	-11.123	0.837
5	500	9.734	9.505	19.629	6.743	-11.078	0.840

performance of the model. Higher R^2 values as well as lower RMSE and nRMSE values suggest the resulting model has higher precision (Yang et al., 2023). nRMSE is a percentage-based metric derived by scaling the RMSE using the population's maximum and minimum values; lower nRMSE values indicate a closer alignment between model predictions and observed data (Arjasakusuma et al., 2020). The optimal model was found at an R^2 value of 0.824 and RMSE of 9.7% with m-try 4 and n-tree 100.

Variable prediction stand volume estimation Among the 19 predictor variables used, those derived from passive sensor imagery were the most important in modeling the volume estimation. The five variables of highest importance were FCD, GEMI, SAVI, also Band 12 and Band 5 from Sentinel-2, as shown in Figure 5. Jensen (2009) explains that the spectral characteristics of reflectance of healthy green vegetation range from 0.4 to 2.6 µm wavelength. The multicollinearity matrix in Figure 6 shows the correlations between multi-sensor image variables in the estimation model processed in raster form and produces spatial correlation. The correlation results between variables show that the FCD transformation and the single backscatter VV are reliable variables having a low level of correlation with other variables. Therefore, using these variables together with others can effectively explain the forest inventory in the modeling.

Estimation of stand volume using random forest Landsat optical imagery, which includes thermal channels, can be used for FCD modeling as an initial classification to obtain field survey data categorized by canopy density. FCD has the capability to provide information about structural composition, while unsupervised classification offers information on two-dimensional canopy cover. Additionally, FCD represents a structural composition derived from several index transformations that minimize the influence of atmospheric conditions, shadows, and soil reflectance, resulting in better data for planning and implementing forest rehabilitation, monitoring forest degradation, and assessing reforestation progress. The integration of FCD, index transformations from Sentinel-2, and multi-polarization combinations from Sentinel-1 at the same location is used as predictor variables, with Random Forest Regression applied to develop an empirical model based on field measurement data and the variables derived from these sources.

In the model, tree diameter and height data were used to calculate the volume at the measuring plot, which was generalized to a size of 30 m². The relationship between volume per plot and FCD transformation is not always linear, as described by Forrester et al. (2018). Selective silviculture systems in production forests also affect the relationship between tree crown density and density, which needs to be taken into account. Therefore, (Sprintsin et al., 2009) described the relationship between canopy and stand density, using both ground-based and satellite methods. The results showed a higher correlation on land with few trees with good canopy growth than those having many small trees (Sprintsin et al., 2009).

Estimation of stand volume using random forest on 30 m^2 plots showed a volume from 0.05 m^3 to 55.4 m^3, spatially presented in Figure 7. The volume estimation variables were most influenced by combination bands in images with passive sensors compared to those from active sensors. In addition to band combination in the form of the SAVI index and FCD model transformation, the volume estimation variable was also influenced by the red edge, and SWIR channel. This is presumably because the red edge channel is highly sensitive to vegetation. The spectral reflectance characteristics of healthy green vegetation for the wavelength interval 0.4–2.6 µm. The dominant factors controlling leaf reflectance are various leaf pigments in the palisade

Jurnal Manajemen Hutan Tropika, *32*(3), 215–228, July 2026
EISSN: 2089-2063
DOI: 10.7226/jtfm.32.3.215
Scientific Article
ISSN: 2087-0469

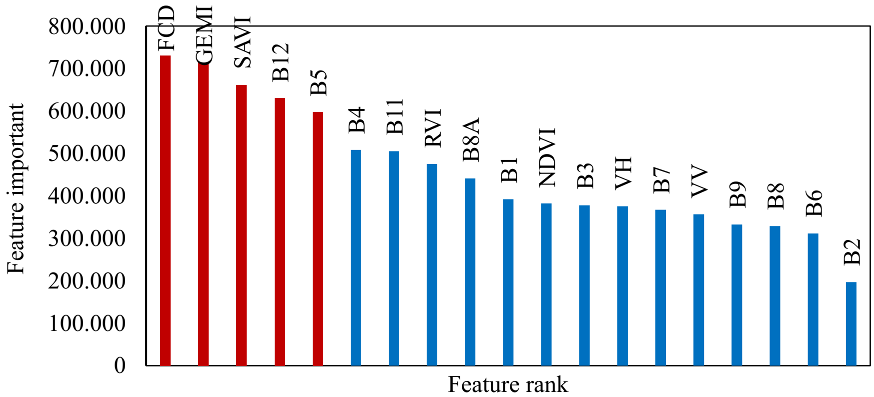

Figure 5 Predicted variables for stand volume estimation.

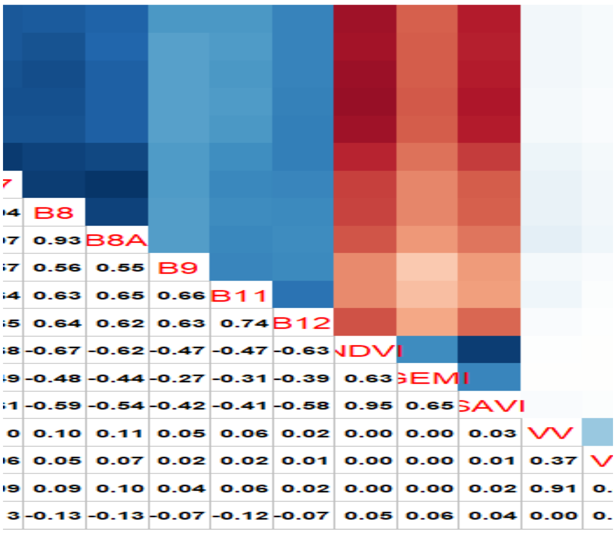

Figure6 Multicollinearity matrix between predictor variables.

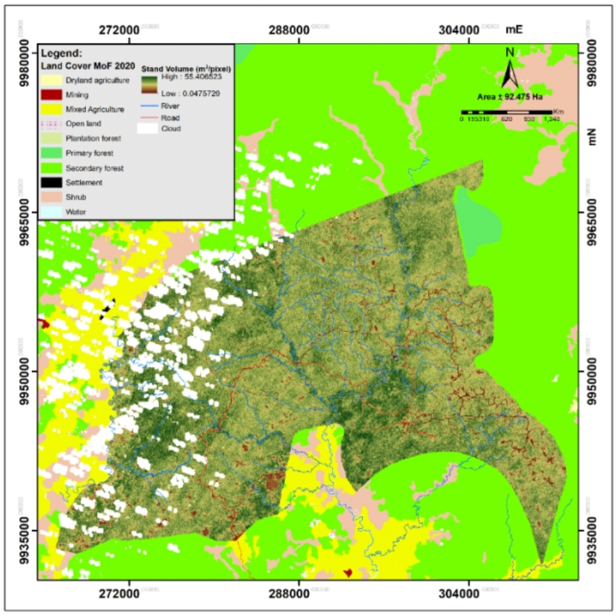

Figure 7 Stand volume map model.

mesophyll (e.g. chlorophyll a and b, and β-carotene), near-infrared energy scattering in the spongy mesophyll, and the amount of water in the plant. Primary chlorophyll uptake occurs at wavelengths of 0.43–0.45 µm and 0.65–0.66 µm in the visible region (Jensen, 2009).

Discussion

Accuracy testing for the correlation between FCD and field data showed identifiable estimation errors, but challenges such as clouds, cloud shadows, and heterogeneous forest conditions need to be addressed in the use of the FCD transformation. This study presents an effective approach for volume estimation by using the FCD model and multi-sensor satellite image-based utilization, which can help forest monitoring and management efficiently.

A vegetation phenology study by Frison et al. (2018), using Sentinel-1A, showed clear differences, reinforcing the potential of data for vegetation monitoring. The SAR backscatter method was also successful in a biomass study conducted in Kalimantan by Berninger et al., although with limitations of signal return in the high biomass range (Berninger et al., 2018). A study by Wijaya et al. (2010) on secondary tropical forests that have experienced succession under logging practices in East Kalimantan Province, Indonesia reported the potential for estimating tree biomass at the scale of logging activities in tropical Dipterocarpaceae forest. Pearson correlations showed that mean texture indices were highly correlated with forest attributes. Furthermore, forest attributes increased with canopy layer development and vegetation complexity, from the simplest to the most complex, and advanced secondary forest (ASF) class (Wijaya et al., 2010).

In this study, the training data used 30 samples of actual volume measurements in the field from previous FCD-transformed density model samples. A regression model was included in supervised learning where there was input x and output y. The task was to learn the mapping from input to output (Budiharto, 2016). Machine learning works by discovering some relationship between features and target variables to validate the performance of training data (training set) with a separate dataset (test set). Therefore, the system decides on each example to perform the task of predicting numerical values. Using 30 training data sets and 19 predictor variables, this study provided a fairly good volume estimation model by adjusting the hyperparameter tuning performed before running the Random Forest Regression model. Hyperparameters are not optimized by the learning algorithm. The user must "tune" the hyper-parameters by experimentally finding the best combination of values, one per hyperparameter. It is important to have enough data for a decent validation set where each class is represented by at least a few data samples. The performance of each model on the validation data was then assessed using an accuracy parameter including RMSE, MAE, or R^2. Overfitting can occur when the model is extremely complex or there are excessive features but a small number in the training set. Some ways to solve the overfitting problem include trying simpler models, reducing the size in the dataset, and adding more samples to the training set (Burkov, 2019). A model is considered to have a low bias when it predicts the training data well. On the other hand, when the model makes many errors in the training data, it has a high bias. Underfitting refers to the inability of the model to excellently predict the training data presumably because the model is too simple for the data or the features are not significantly informative.

These results demonstrate the reliability and accuracy of the model in estimating stand volume in the area, showing that the combination of FCD transformations, Sentinel-1A imagery, and Sentinel-2 indices can be an effective tool for monitoring and estimating forest health. By optimizing the use of images with acquisition dates close to field activities and increasing the amount of training data, the model can be replicated in similar forest conditions.

Conclusion

This study demonstrates the applicability of multi-sensor remote sensing and Random Forest Regression for estimating stand volume in natural production forests. The FCD model proved effective in stratifying canopy density, showing a significant correlation with field-measured canopy cover ($R^2 = 0.76$), although its reliability was affected by temporal discrepancies and structural changes in forest conditions. Among the 19 tested predictors, the most accurate model performance ($R^2 = 0.824$; RMSE = 9.7) was achieved using only four key variables: FCD transformation, GEMI, SAVI, and Sentinel-2 bands 5 and 12. Stand volume estimation was efficiently achieved using a minimal set of variables, with stratified random sampling based on FCD-derived canopy classes across 70 field plots revealing volumes ranging from 0.05 m^3 $pixel^{-1}$ to 55.4 m^3 $pixel^{-1}$.

Recommendation

For future research, it is recommended to use imagery with acquisition dates closely aligned with field data collection to minimize temporal discrepancies, particularly when applying the FCD model in heterogeneous stands managed through selective silvicultural systems. Additionally, increasing the sample size is essential to enhance the predictive accuracy of stand volume models using the random forest algorithm. The proposed volume estimation approach is also more suitable for production forests employing THPB (clear-cut artificial propagation) systems, such as those in pulp and paper plantations, due to the distinct spatial patterns visible in remote sensing imagery. Furthermore, focusing field measurements on commercial tree species can improve data quality for operational logging planning.

Acknowledgment

The author is grateful to the Faculty of Geography, Gadjah Mada University, specifically the Remote Sensing Program and PBPH-PT Wana Inti Kahuripan Intiga for data support and assistance with field data collection in the study area. Furthermore, appreciation goes to the Ministry of Finance of Indonesia for the Education Fund Management Agency scholarship.

References

Abdollahnejad, A., Panagiotidis, D., & Surový, P. (2017). Forest canopy density assessment using different approaches-Review. *Journal of Forest Science*, *63*(3), 107–116. https://doi.org/10.17221/110/2016-JFS

Arjasakusuma, S., Kusuma, S. S., & Phinn, S. (2020). Evaluating variable selection and machine learning algorithms for estimating forest heights by combining lidar and hyperspectral data. *ISPRS International Journal of Geo-Information*, *9*(9), Article 507. https://doi.org/10.3390/ijgi9090507

Ataee, M. S., Maghsoudi, Y., Latifi, H., & Fadaie, F. (2019). Improving estimation accuracy of growing stock by multi-frequency SAR and multi-spectral data over Iran's heterogeneously-structured broadleaf Hyrcanian forests. *Forests*, *10*(8), Article 641. https://doi.org/10.3390/f10080641

Bannari, A., Morin, D., Bonn, F., & Huete, A. R. (1995). A review of vegetation indices. *Remote Sensing Reviews*, *13*(1–2), 95–120. https://doi.org/10.1080/027572595 09532298

Berninger, A., Lohberger, S., Stängel, M., & Siegert, F. (2018). SAR-based estimation of above-ground biomass and its changes in tropical forests of Kalimantan using L- and C-band. *Remote Sensing*, *10*(6), Article 831. https://doi.org/10.3390/rs10060831

Brede, B., Bartholomeus, H. M., Barbier, N., Pimont, F., Vincent, G., & Herold, M. (2022). Peering through the thicket: Effects of UAV LiDAR scanner settings and flight planning on canopy volume discovery. *International Journal of Applied Earth Observation and Geoinformation*, *114*, Article 103056. https://doi.org/10.1016/j.jag.2022.103056

Breiman, L. (2001). Random forests. *Machine Learning*, *45*, 5–32. https://doi.org/10.1023/A:1010933404324

Budiharto, W. (2016). *Machine learning and computational intelligence*. Yogyakarta: Andi.

Burkov, A. (2019). *The hundred-page machine learning book*. Andriy Burkov Publ.

Congalton, R. G., & Green, K. (2019). *Assessing the accuracy of remotely sensed data: Principles and practices* (3rd ed.). CRC Press. https://doi.org/10.1201/9780429052729

Danoedoro, P. (2012). *Pengantar penginderaan jauh digital*. Yogyakarta: Andi.

Díaz, G. M. (2023). Optimizing forest canopy structure retrieval from smartphone-based hemispherical photography. *Methods in Ecology and Evolution*, *14*(3), 875–884. https://doi.org/10.1111/2041-210X.14059

Esteban, J., McRoberts, R. E., Fernández-Landa, A., Tomé, J. L., & Næsset, E. (2019). Estimating forest volume and biomass and their changes using random forests and remotely sensed data. *Remote Sensing*, *11*(16), Article 1944. https://doi.org/10.3390/rs11161944

Forrester, D. I., Ammer, C., Annighöfer, P. J., Barbeito, I., Bielak, K., Bravo-Oviedo, A., Coll, L., del Río, M., Drössler, L., Heym, M., Hurt, V., Löf, M., den Ouden, J., Pach, M., Pereira, M. G., Plaga, B. N. E., Ponette, Q., Skrzyszewski, J., Sterba, H., …, & Pretzsch, H. (2018). Effects of crown architecture and stand structure on light absorption in mixed and monospecific *Fagus sylvatica* and *Pinus sylvestris* forests along a productivity and climate gradient through Europe. *Journal of Ecology*, *106*(2), 746–760. https://doi.org/10.1111/1365-2745.12803

Frazer, G. W., Canham, C. D., & Lertzman, K. P. (1999). *Gap light analyzer (GLA). Imaging software to extract canopy structure and gap light transmission indices from true-colour fisheye photographs. User manual and program documentation, version 2.0.* Simon Fraser University, Burnaby, British Columbia-the Institute of Ecosystem Studies, Millbrook, New York.

Frison, P. L., Fruneau, B., Kmiha, S., Soudani, K., Dufrêne, E., Le Toan, T., Koleck, T., Villard, L., Mougin, E., & Rudant, J. P. (2018). Potential of Sentinel-1 data for monitoring temperate mixed forest phenology. *Remote Sensing*, *10*(12), Article 2049. https://doi.org/10.3390/rs10122049

Ghorbanian, A., Zaghian, S., Asiyabi, R. M., Amani, M., Mohammadzadeh, A., & Jamali, S. (2021). Mangrove ecosystem mapping using Sentinel-1 and Sentinel-2 satellite images and random forest algorithm in google earth engine. *Remote Sensing*, *13*(13), 1–18. https://doi.org/10.3390/rs13132565

Giertych, M. J., Karolewski, P., & Oleksyn, J. (2015). Carbon allocation in seedlings of deciduous tree species depends on their shade tolerance. *Acta Physiologiae Plantarum*, *37*(216), 1–15. https://doi.org/10.1007/s11738-015-1965-x

Giri Ananto, W. H., Hadi, H. A., Sandhini Putri, A. F., Hanum, D. N., Puji Wiryawan, B. K., Prabaswara, R. R., & Arjasakusuma, S. (2019). Assessment of dual polarization in Sentinel-1 data for estimating forest aboveground biomass: Case study of Barru Regency, South Sulawesi. *Proceedings Sixth International Symposium on LAPAN-IPB Satellite*, *11372*, Article 1137214. https://doi.org/10.1117/12.2540845

González-Alonso, F., Merino-De-Miguel, S., Roldán-Zamarrón, A., García-Gigorro, S., & Cuevas, J. M. (2006). Forest biomass estimation through NDVI composites. The role of remotely sensed data to assess Spanish forests as carbon sinks. *International Journal of Remote Sensing*, *27*(24), 5409–5415. https://doi.org/10.1080/01431160600830748

Heriansyah, I., Hamid, H. A., Nurudin, A. A., Ibrahim, S., Abdu, A., & Alias, M. A. (2022). Assessment of reduced impact logging technique at different logging intensity. *IOP Conference Series: Earth and Environmental Science*, *959*, Article 012067. https://doi.org/10.1088/1755-1315/959/1/012067

Himayah, S., Hartono, & Danoedoro, P. (2016). The utilization of Landsat 8 multitemporal imagery and forest canopy density (FCD) model for forest reclamation rriority of natural disaster areas at Kelud Mountain, East Java. *IOP Conference Series: Earth and Environmental Science*, *47*, Article 012043. https://doi.org/10.1088/1755-1315/47/1/012043

Huete, A. R. (1988). A soil-adjusted vegetation index (SAVI). *Remote Sensing of Environment*, *25*(3), 295–309. https://doi.org/10.1016/0034-4257(88)90106-X

Iizuka, K., Hayakawa, Y. S., Ogura, T., Nakata, Y., Kosugi, Y., & Yonehara, T. (2020). Integration of multi-sensor data to estimate plot-level stem volume using machine learning algorithms-case study of evergreen conifer planted forests in Japan. *Remote Sensing*, *12*(10), Article 1649. https://doi.org/10.3390/rs12101649

Ismail, M., Hartono, & Danoedoro, P. (2017). The application of forest cover density (FCD) model for structural composition of vegetation changes in part of Lore Lindu National Park, Central Sulawesi Province. *IOP Conference Series: Earth and Environmental Science*, *98*, Article 012056. https://doi.org/10.1088/1755-1315/98/1/012056

Jensen, J. R. (2009). *Remote Sensing of the environment, an earth resource perspective* (2nd ed.). Pearson Education.

Kalkhan, M. A. (2011). *Spatial statistics. GeoSpatial information modelling and thematic mapping*. CRC Press, Taylor & Francis Group. https://doi.org/10.1201/

9781439891117

Kuchler, A.W. & Zonnevald, I. S. (Eds.). (1988). *Vegetation mapping* (Handbook of vegetation science, 10). Kluwer Academic Publishers.

Kumar, S. D., Rao, S. S., & Sharma, J. R. (2013). Radar vegetation ias an alternative to NDVI for monitoring of soyabean and cotton. *Indian Cartographer*, *33*, 91–96.

Manan, F. A., Saleh, M. B., Jaya, I. N. S., & Mukarom, U. S. (2019). Algorithm for assessing forest stand productivity index using leaf area index. *Indonesian Journal of Electrical Engineering and Computer Science*, *16*(3), 1311–1319. https://doi.org/10.11591/ijeecs.v16.i3.pp1311-1319

Mas Sukarna, R., & Syahid, Y. (2015). FCD application of Landsat for monitoring mangrove in Central Kalimantan. *Indonesian Journal of Geography*, *47*(2), 160–170. https://doi.org/10.22146/ijg.9259

McCoy, R. M. (2005). *Field methods in remote sensing*. Kluwer Academic Publishers. http://doi.wiley.com/10.1111/j.1541- 0064.2006.00161_2.x

Medasani, S, & Reddy, G. U. (2018). Analysis and evaluation of speckle filters by using polarimetric synthetic aperture radar data through local statistics. In *2018 second international conference on electronics, communication and aerospace technology* (pp. 169–174). Coimbatore, India. https://doi.org/10.1109/ICECA.2018.8474567

Mullissa, A., Vollrath, A., Odongo-Braun, C., Slagter, B., Balling, J., Gou, Y., Gorelick, N., & Reiche, J. (2021). Sentinel-1 SAR backscatter analysis ready data preparation in Google Earth Engine. *Remote Sensing*, *13*(10) Article 1954. https://doi.org/10.3390/rs13101954

Nasiri, V., Sadeghi, S. M. M., Moradi, F., Afshari, S., Deljouei, A., Griess, V. C., Maftei, C., & Borz, S. A. (2022). The influence of data density and integration on forest canopy cover mapping using Sentinel-1 and Sentinel-2 time series in Mediterranean Oak Forests. *ISPRS International Journal of Geo-Information*, *11*(8), Article 423. https://doi.org/10.3390/ijgi11080423

Nasirzadehdizaji, R., Sanli, F. B., Abdikan, S., Cakir, Z., Sekertekin, A., & Ustuner, M. (2019). Sensitivity analysis of multi-temporal Sentinel-1 SAR parameters to crop height and canopy coverage. *Applied Sciences*, *9*(4), Article 655. https://doi.org/10.3390/app9040655

Kementerian Lingkungan Hidup dan Kehutanan. (2021). *Peraturan Menteri Nomor 8 Tahun 2021 tentang Tata Hutan dan Penyusunan Rencana Pengelolaan Hutan, serta Pemanfaatan Hutan di Hutan Lindung dan Hutan Produksi*. Peraturan.go.id. https://peraturan.go.id/id/permen-lhk-no-8-tahun-2021

Pinty, B., & Verstraete, M. M. (1992). GEMI: A non-linear index to monitor global vegetation from satellites. *Vegetatio*, *101*(1), 15–20. https://doi.org/10.1007/BF00031911

Rao, K. V. R. (2023). Removal of speckle noise from SAR images using various filters. *International Journal Of Engineering Research & Technology*, *12*(5), 135–141. https://doi.org/10.17577/IJERTV12IS050043

Rikimaru, A., Roy, P. S., & Miyatake, S. (2002). Tropical forest cover density mapping. *International Society Tropical Ecology*, *43*(1), 39–47.

Rondeaux, G., Steven, M., & Baret, F. (1996). Optimization of soil-adjusted vegetation indices. *Remote Sensing of Environment*, *55*(2), 95–107. https://doi.org/10.1016/0034-4257(95)00186-7

Roy, P. S., Miyatake, S., & Rikimaru, A. (1997). Biophysical spectral response modeling approach for forest density stratification. *Geospatial World.* Retrieved from https://geospatialworld.net/article/biophysical-spectral-response-modeling-approach-for-forest-density-stratification/

Salsabila, H. N., & Danoedoro, P. (2021, November 22–24). *Comparing two diffferent radiometric corrections in a vegetation mapping of mountainous area using forest canopy density transformation* [Conference presentation]. *The 42nd Asian Conference on Remote Sensing ACRS 2021*, Can Tho city, Vietnam.

Schratz, P., Muenchow, J., Iturritxa, E., Richter, J., & Brenning, A. (2019). Hyperparameter tuning and performance assessment of statistical and machine-learning algorithms using spatial data. *Ecological Modelling*, *406*, 109–120. https://doi.org/10.1016/j.ecolmodel.2019.06.002

Shehzad, K., Anwar, A., Samia, A., Areeba, B. I., & Naveed, A. (2022). Mapping and monitoring forest landscape restoration using Landsat-8 images. *Bulletin of the Transilvania University of Brasov, Series II: Forestry, Wood Industry, Agricultural Food Engineering*, *15–64*(2), 43–64. https://doi.org/10.31926/but.fwiafe.2022.15.64.2.4

Sprintsin, M., Karnieli, A., Sprintsin, S., Cohen, S., & Berliner, P. (2009). Relationships between stand density and canopy structure in a dryland forest as estimated by ground-based measurements and multi-spectral spaceborne images. *Journal of Arid Environments*, *73*(10), 955–962. https://doi.org/10.1016/j.jaridenv.2009.04.011

Sukarna, R. M. (2008). Aplikasi forest canopy density citra Landsat 7 ETM untuk menentukan luas tajuk (crown areal index) dan kerapatan tegakan (stand density) hutan rawa gambut di DAS Sebangau Provinsi Kalimantan Tengah. *Majalah Geografi Indonesia*, *22*(1), 1–21.

Szigarski, C., Jagdhuber, T., Baur, M., Thiel, C., Parrens, M., Wigneron, J. P., Piles, M., & Entekhabi, D. (2018). Analysis of the radar vegetation index and potential improvements. *Remote Sensing*, *10*(11), Article 1776. https://doi.org/10.3390/rs10111776

Umarhadi, D. A., & Danoedoro, P. (2020). The effect of topographic correction on canopy density mapping using satellite imagery in mountainous area. *International Journal on Advanced Science, Engineering and Information Technology*, *10*(3), 1317–1325. https://doi.org/10.18517/ijaseit.10.3.7739

Villarroya-Carpio, A., Lopez-Sanchez, J. M., & Engdahl, M. E. (2022). Sentinel-1 interferometric coherence as a vegetation index for agriculture. *Remote Sensing of Environment*, *280*, Article 113208. https://doi.org/10.1016/j.rse.2022.113208

Vollrath, A., Mullissa, A., & Reiche, J. (2020). Angular-based radiometric slope correction for Sentinel-1 on google earth engine. *Remote Sensing*, *12*(11), Article 1867. https://doi.org/10.3390/rs12111867

Wijaya, A., Liesenberg, V., & Gloaguen, R. (2010). Retrieval of forest attributes in complex successional forests of Central Indonesia: Modeling and estimation of bitemporal data. *Forest Ecology and Management*, *259*(12), 2315–2326. https://doi.org/10.1016/j.foreco.2010.03.004

Wittke, S., Yu, X., Karjalainen, M., Hyyppä, J., & Puttonen, E. (2019). Comparison of two-dimensional multitemporal Sentinel-2 data with three-dimensional remote sensing data sources for forest inventory parameter estimation over a boreal forest. *International Journal of Applied Earth Observation and Geoinformation*, *76*, 167–178. https://doi.org/10.1016/j.jag.2018.11.009

Yadav, V. P., Prasad, R., Bala, R., Srivastava, P. K., & Vanama, V. S. K. (2022). Appraisal of dual polarimetric radar vegetation index in first order microwave scattering algorithm using Sentinel-1A (C-band) and ALOS-2 (L-band) SAR data. *Geocarto International*, *37*(21), 6232–6250. https://doi.org/10.1080/10106049.2021.1933209

Yang, S., Feng, Q., Yang, W., & Gao, X. (2023). Simple, low-cost estimation of potato above-ground biomass using improved canopy leaf detection method. *American Journal of Potato Research*, *100*, 143–162. https://doi.org/10.1007/s12230-022-09897-w

Yu, Z., Wang, W., Li, C., Liu, W., & Yang, J. (2018). Speckle noise suppression in SAR images using a three-step algorithm. *Sensors*, *18*(11). Article 3643. https://doi.org/10.3390/s18113643

Zhu, X., & Liu, D. (2015). Improving forest aboveground biomass estimation using seasonal Landsat NDVI time-series. *ISPRS Journal of Photogrammetry and Remote Sensing*, *102*, 222–231. https://doi.org/10.1016/j.isprsjprs.2014.08.014